Langmuir Article

pubs.acs.org/Langmuir

Fouling Behavior of Microstructured Hollow Fiber Membranes in Dead-End Filtrations: Critical Flux Determination and NMR Imaging of Particle Deposition

P. Zeynep Çulfaz,[†,‡] Steffen Buetehorn,[§] Lavinia Utiu,[∥] Markus Kueppers,[∥] Bernhard Bluemich,[∥] Thomas Melin,[§] Matthias Wessling,[§,‡] and Rob G. H. Lammertink*[,†]

[†]*Soft Matter, Fluidics and Interfaces,* [‡]*Membrane Technology Group, Mesa+ Institute for Nanotechnology University of Twente, P.O. Box 217, 7500AE, Enschede, The Netherlands,* [§]*Chemical Process Engineering-AVT.CVT, and* [∥] *Macromolecular Chemistry-ITMC, RWTH Aachen University, 52056 Aachen, Germany*

Received September 20, 2010. Revised Manuscript Received November 13, 2010

The fouling behavior of microstructured hollow fibers was investigated in constant flux filtrations of colloidal silica and sodium alginate. It was observed that the fouling resistance increases faster with structured fibers than with round fibers. Reversibility of structured fibers' fouling was similar during silica filtrations and better in sodium alginate filtrations when compared with round fibers. The deposition of two different silica sols on the membranes was observed by NMR imaging. The sols had different particle size and solution ionic strength and showed different deposition behaviors. For the smaller particle-sized sol in deionized solution (Ludox-TMA), there was more deposition within the grooves of the structured fibers and much less on the fins. For the alkali-stabilized sol Bindzil 9950, which had larger particles, the deposition was homogeneous across the surface of the structured fiber, and the thickness of the deposit was similar to that on the round fiber. This difference between the deposition behavior of the two sols is explained by differences in the back diffusion, which creates concentration polarization layers with different resistances. The Ludox sol formed a thick polarization layer with very low resistance. The Bindzil sol formed a slightly thinner polarization layer; however, its resistance was much higher, of similar magnitude as the intrinsic membrane resistance. This high resistance of the polarization layer during the Bindzil sol filtration is considered to lead to quick flow regulation toward equalizing the resistance along the fiber surface. The Ludox particles were trapped at the bottom of the grooves as a result of reduced back diffusion. The fouling behavior in sodium alginate filtrations was explained by considering the size-dependent deposition within the broad alginate size distribution. The better reversibility of fouling in the structured fibers is thought to be the result of a looser deposit within the grooves, which is more easily removed than a compressed deposit on the round fibers.

Introduction

Concentration polarization and succeeding particle deposition on the membrane surface are the main factors limiting the productivity of membranes.[1−3] Concentration polarization is inherent to all membrane separations because it is a result of the accumulation of retained material near the membrane surface. For colloids (1−1000 nm), when the particle concentration near the membrane exceeds a certain value, the particles coagulate to form a cake or gel layer.[4,5] This phase transition from the dispersed phase to the condensed phase is due to the surface interactions between the particles and depends strongly on solution properties such as pH and ionic strength as well as the size and surface charge of the colloidal particles.[6]

Membrane filtrations can be operated in dead-end or cross-flow modes. The choice depends on the optimization of the productivity versus the operational costs. For heavily fouling feeds, cross-flow is often necessary, whereas for feeds with lower fouling potential, dead-end operation is usually more economical. In a dead-end filtration, the retained particles continuously accumulate on the membrane surface as filtration proceeds. To prevent excessive performance decline, periodic backwashes are required to remove deposited particles from the membrane surface. For sustainable operation, the backwashing should be able to remove all of the deposited particles, in which case the deposition on the membrane is classified as reversible fouling. Any irreversible fouling will deteriorate the membrane's performance in time and is therefore undesired. In a dead-end filtration, the flux below which all fouling is reversible is defined as the "critical flux".[7,8] The critical flux for a certain membrane depends on the feed solution and the filtrate load between two backwashes.

*To whom correspondence should be addressed. E-mail: r.g.h.lammertink@utwente.nl.

(1) Chen, V.; Fane, A. G.; Madaeni, S.; Wenten, I. G. Particle deposition during membrane filtration of colloids: Transition between concentration polarization and cake formation. *J. Membr. Sci.* **1997**, *125*, 109–122.

(2) Elimelech, M.; Bhattacharjee, S. A novel approach for modeling concentration polarization in crossflow membrane filtration based on the equivalence of osmotic pressure model and filtration theory. *J. Membr. Sci.* **1998**, *145*, 223–241.

(3) Goosen, M. F. A.; Sablani, S. S.; Al-Hinai, H.; Al-Obeidani, S.; Al-Belushi, R.; Jackson, D. Fouling of reverse osmosis and ultrafiltration membranes: A critical review. *Sep. Sci. Technol.* **2004**, *39*, 2261–2297.

(4) Bacchin, P.; Meireles, M.; Aimar, P. Modelling of filtration: from the polarised layer to deposit formation and compaction. *Desalination* **2002**, *145*, 139–146.

(5) Jönsson, A.; Jönsson, B. Ultrafiltration of colloidal dispersions - a theoretical model of the concentration polarization phenomena. *J. Colloid Interface Sci.* **1996**, *180*, 504–518.

(6) Bacchin, P.; Si-Hassen, D.; Starov, V.; Clifton, M. J.; Aimar, P. A unifying model for concentration polarization, gel-layer formation and particle deposition in cross-flow membrane filtration of colloidal suspensions. *Chem. Eng. Sci.* **2002**, *57*, 77–91.

(7) Bessiere, Y.; Abidine, N.; Bacchin, P. Low fouling conditions in dead-end filtration: evidence for a critical filtered volume and interpretation using critical osmotic pressure. *J. Membr. Sci.* **2005**, *264*, 37–47.

(8) van de Ven, W. J. C.; van't Sant, K.; Pünt, I. G. M.; Zwijnenburg, A.; Kemperman, A. J. B.; van der Meer, W. G. J.; Wessling, M. Hollow fiber dead-end ultrafiltration: Influence of ionic environment on filtration of alginates. *J. Membr. Sci.* **2008**, *308*, 218–229.

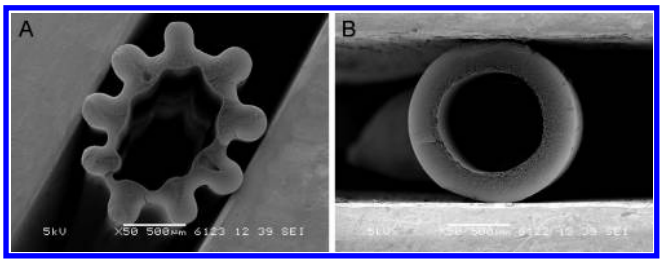

Figure 1. (a) Microstructured and (b) round hollow fibers used in this study.

For the study of fouling, the first approach is to monitor the transmembrane pressure increase at constant flux or flux decline at constant pressure and to determine the reversibility of the fouling. Complementary to these indirect methods of fouling detection, in recent years, there have been efforts to observe particle deposition on membranes in situ.[9] One of these methods is NMR imaging, which is able to identify local concentration variations. The method has been used to visualize the formation of polarization layers during the filtration of oil−water emulsions, bentonite, and colloidal silica particles.[10,11] In bentonite and silica suspensions, the particles do not contribute to the NMR signal, but they alter the relaxation times (T_1 and T_2) of surrounding water protons. By relating the particle concentration to T_1 and T_2, information on concentration polarization and particle deposition can be obtained.

In this study, we characterize the fouling behavior of microstructured hollow fiber membranes in dead-end filtrations by using both critical flux determination methods and online NMR imaging of particle deposition. In our previous study, these microstructured membranes were shown to increase the productivity by increasing the membrane area per fiber length compared with round fibers.[12] The characterization of the fouling behavior of these membranes in dead-end systems provides insight into the productivity of these membranes in actual filtrations as well as a starting point for understanding filtrations in cross-flow and submerged, aerated systems.

Experimental Section

Membranes. One microstructured and one round hollow fiber membrane made by the dry−wet phase inversion of the polymer dope 16.68% PES, 4.91% PVP K30, 4.91% PVP K90, 7.18% H_2O, and 66.32% NMP, with water as the external coagulant, were used throughout this study (Figure 1). Details of the fabrication are described elsewhere.[12] The structured fiber has 60% higher surface area per length compared with the round fiber. The pure water permeabilities of the fibers are 235 ± 11 and 233 ± 12 L/h·m^2·bar for structured and round fibers, respectively. The mean pore diameter of both fibers was found to be 12 nm by permporometry measurements (Figure 2). The skin layer thicknesses of the fibers were determined using a colloidal filtration method described in a previous study.[12] The skin layer of the structured fiber was found to have homogeneous thickness all throughout the surface and to be equally thick as that of the round fiber (1.5 μm).

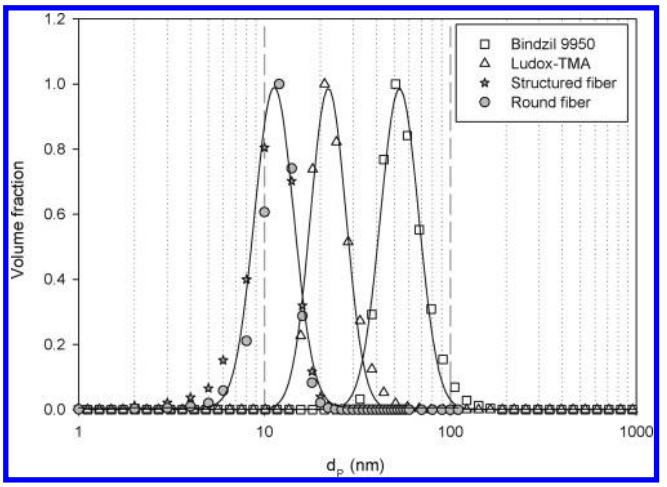

Figure 2. Particle size distributions of the silica sols and the pore size distributions of the membranes.

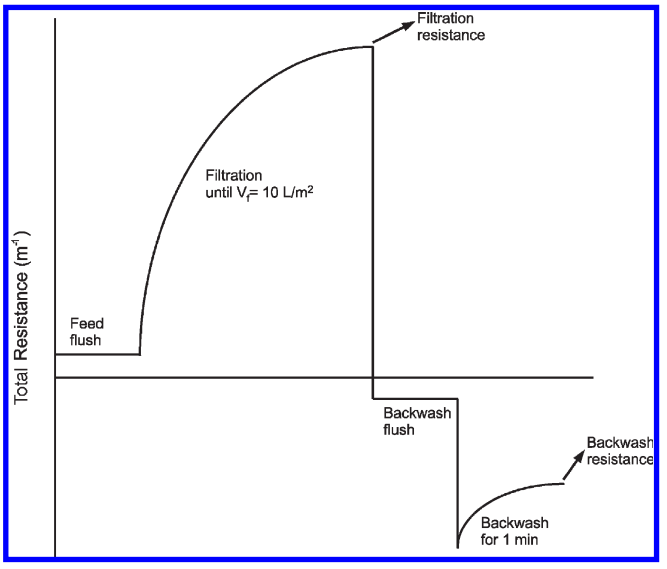

Figure 3. Single cycle used in flux-stepping experiments consisting of filtration and backwash.

Consequently, any difference in fouling behavior observed between the structured and round fibers is attributed to the difference in the microstructure of the outer surfaces and not due to the intrinsic properties of the membranes.

Materials. Ludox-TMA colloidal silica was purchased from Sigma-Aldrich. The stock solution has 34 wt % silica in deionized water with pH of 6 to 7. Bindzil-9950 colloidal silica was kindly provided by Eka Akzo Nobel. The stock solution contains 50 wt % silica and is alkali-stabilized at a pH of 9. The particle size distribution and zeta potential of the sols were measured with a Malvern Zetasizer Nano-ZS instrument. The particle size distributions of the sols are shown in Figure 2 together with the pore size distribution of the membranes measured by permporometry. Although there is a small overlap between the particle size distribution of Ludox-TMA and the pore size distribution of the membranes, no silica was observed in the permeates.

Sodium alginate (A2158, low viscosity, ~ 250 cP at 2%) was purchased from Sigma-Aldrich. All feed solutions were prepared with ultrapure water (18 mΩ·cm). The retention of sodium alginate was determined by total carbon analysis using TOC−V_{CPH} (Shimadzu).

Flux-Stepping Experiments. The experimental setup used in the flux-stepping experiments was described in the work of

(9) Chen, V.; Li, H.; Fane, A. G. Non-invasive observation of synthetic membrane processes - a review of methods. *J. Membr. Sci.* **2004**, *241*, 23–44.
(10) Airey, D.; Yao, S.; Wu, J.; Chen, V.; Fane, A. G.; Pope, J. M. An investigation of concentration polarization phenomena in membrane filtration of colloidal silica suspensions by NMR micro-imaging. *J. Membr. Sci.* **1998**, *145*, 145–158.
(11) Yao, S.; Costello, M.; Fane, A. G.; Pope, J. M. Non-invasive observation of flow profiles and polarisation layers in hollow fibre membrane filtration modules using NMR micro-imaging. *J. Membr. Sci.* **1995**, *99*, 207–216.
(12) Çulfaz, P. Z.; Rolevink, E.; van Rijn, C.; Lammertink, R. G. H.; Wessling, M. Microstructured hollow fibers for ultrafiltration. *J. Membr. Sci.* **2009**, *347*, 32–41.

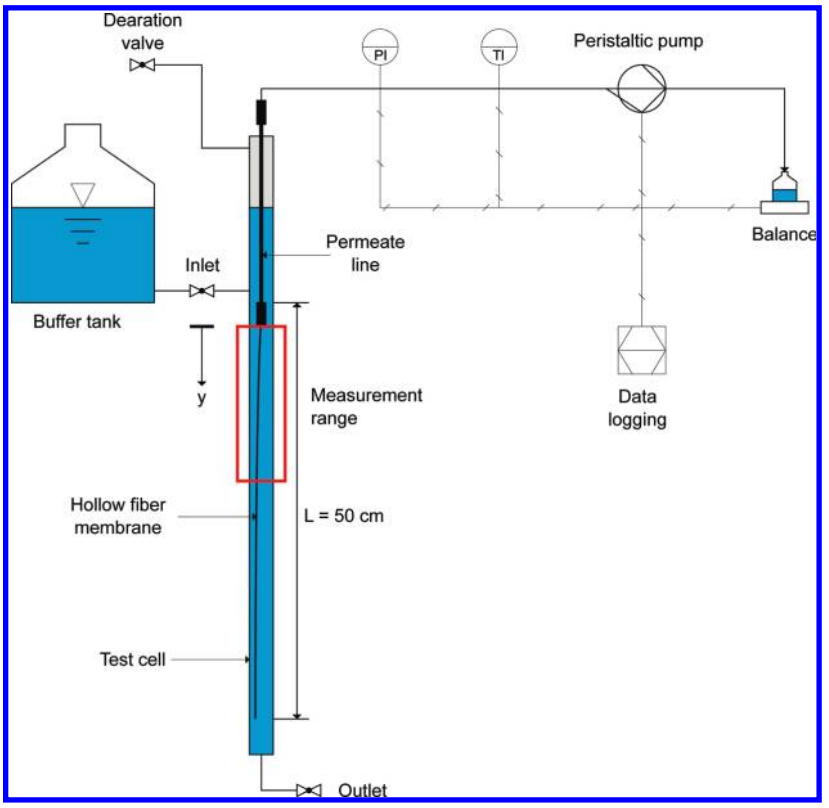

Figure 4. Schematic of the NMR setup.[13]

van de Ven et al.[8] Flux steps from 20 L/h·m^2 to 90 or 110 L/h·m^2 were applied, with 15 cycles at each flux consisting of a filtration period, followed by a backwashing period (Figure 3). The filtration period was carried out until 10 L of permeate was filtered per square meter of membrane area. Backwashing was done for 1 min at 200 L/h·m^2 for the silica feed and 175 L/h·m^2 for the sodium alginate feed. We assessed fouling reversibility by comparing the filtration resistance or backwash resistance (Figure 3) of consequent cycles at constant flux.

Nuclear Magnetic Resonance Imaging. The particle deposition on the surface of the hollow fibers was noninvasively investigated by means of nuclear magnetic resonance (NMR) imaging. For this purpose, the experimental setup shown in Figure 4 was used. The system was equipped with a single hollow fiber of 50 cm length and operated at constant permeate flux. The pressure and the temperature were measured in the permeate line for monitoring the evolution of the fouling resistance over time. A number of consecutive NMR measurements was performed to capture the corresponding increase in cake layer thickness within three adjacent measurement slices. The center lines of these slices were located 5, 10, and 15 mm below the point of permeate extraction at the fiber top. A virgin membrane and a fresh silica suspension were used for each test run. For the silica filtration tests, a transmembrane pressure difference (TMP) of 800 mbar was chosen as an abort criterion. Details of the experimental setup and the test protocols used are explained elsewhere.[13]

The NMR measurements presented in this article are a follow-up of previous studies to visualize cake growth and removal in membrane filtration processes.[13,14] For the observation of cake layers consisting of colloidal silica particles, a 3D gradient echo pulse sequence was applied.[14] Because it is known that the silica particles do not contribute to the ^{1}H NMR signal,[10] a proper cake−bulk contrast was facilitated. This image contrast is due to differences in the relaxation time of water protons bounded to the silica particles as compared with that of free water protons. Within these images, the bulk phase is characterized by a relatively low signal intensity, whereas the signal originating from the cake is higher because of a higher solid concentration. The liquid within the membrane pores appears as a region of lower signal intensity due to the saturation of the free water signal. The membrane lumen, instead, is represented by a bright white spot, which is an image artifact caused by the permeate flow. Alterations in the shape of this spot as the filtration progresses can be attributed to the passage of degassing products during data acquisition. The NMR settings are summarized in Table 1, whereas a more detailed description of the pulse sequence can be found elsewhere.[14]

Table 1. NMR Settings for Cake Growth Visualization[14]

NMR settings	cake growth pulse sequence
sequence type	3D gradient echo
data acquisition time (mm:ss)	03:25
repetition time (TR) (ms)	100
echo time (TE) (ms)	3
flip angle (deg)	45
number of images averaged	8
field of view (FOV) (mm × mm × mm)	9 × 9 × 2
matrix size before zero-filling (pix × pix × pix)	256 × 256 × 1
matrix size after zero-filling (pix × pix × pix)	512 × 512 × 1
spatial resolution before zero-filling (μm)	35.2 (radial direction)
spatial resolution after zero-filling (μm)	17.6 (radial direction)

Results and Discussion

Flux-Stepping Experiments with Colloidal Silica. Figure 5 shows the membrane resistance at the end of the filtration and

(13) Buetehorn, S., Utiu, L., Kueppers, M., Bluemich, B., Wintgens, T., Wessling, M., Melin, T. Non-invasive observation of permeate flux distribution and local cake growth in submerged microfiltration processes via nuclear magnetic resonance (NMR) imaging. Submitted.

(14) Utiu, L. Functional NMR and MRI for Analysis of Materials. Ph.D. Thesis, RWTH Aachen University, 2011.

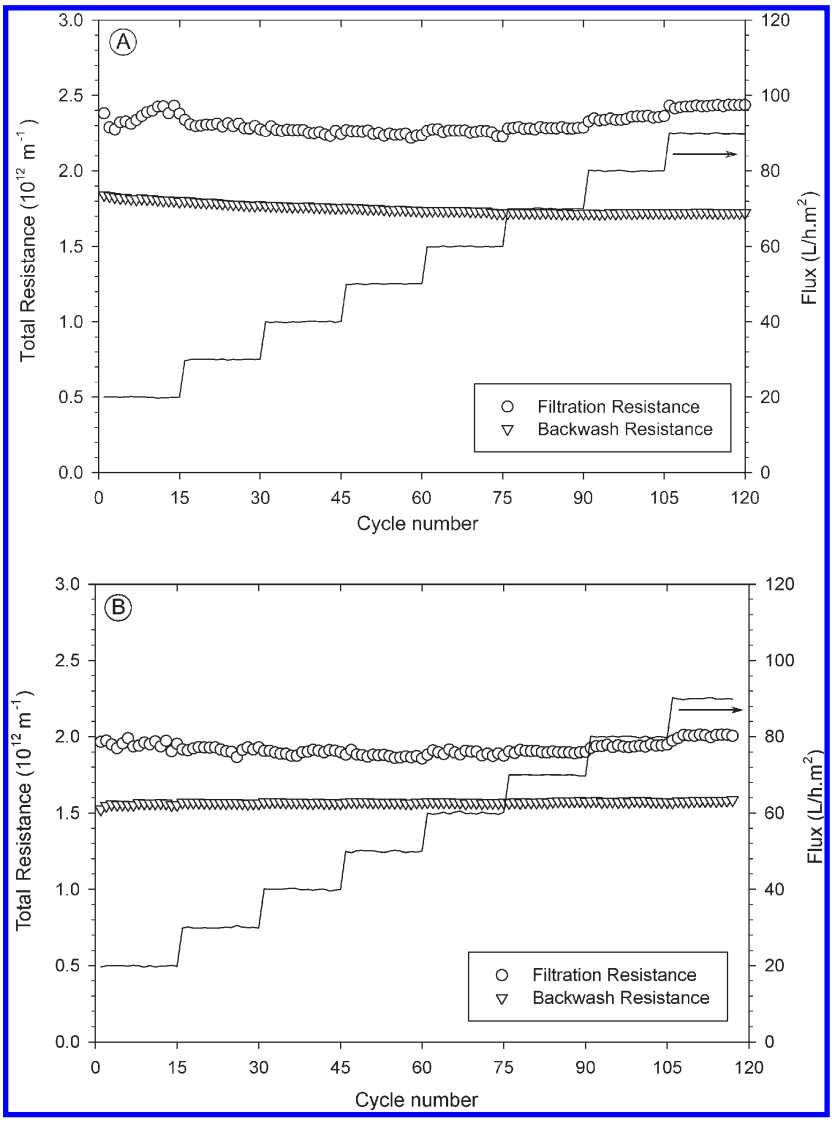

Figure 5. Flux-stepping experiments with 0.05 wt % Ludox-TMA colloidal silica feed: (a) structured fibers and (b) round fibers.

backwash periods (as illustrated in Figure 3) in the flux-stepping experiments with 0.05 wt % Ludox-TMA colloidal silica feed. Both of these resistances were essentially constant in the filtrations at all fluxes during the experiments, implying that there is no significant irreversible fouling in either the structured or the round fibers between fluxes of 20−90 L/h·m^2. In addition, the backwash resistances were close to the intrinsic membrane resistances of the fibers, which also implies that by the end of the backwash, all of the deposit from the filtration period is removed from the membrane surface.

Figure 6 shows the increasing fouling resistance as a function of filtered permeate volume for the structured and round fibers with 0.05 and 0.1 wt % feeds at a flux of 70 L/h·m^2. The resistance increase during the filtrations was steeper for the structured fibers compared with the round ones at all fluxes. The rate of resistance increase ($dR_{fouling}/dV_{filtered}$) also increased with increasing permeate flux for both of the fibers. For the structured fibers, this increase was steeper (Figure 7).

NMR Imaging of Silica Deposition. NMR imaging of particle deposition was carried out with two different kinds of colloidal silica: Ludox-TMA, which was also used in flux-stepping experiments, and Bindzil 9950. As shown in Figure 2, the Ludox-TMA sol has smaller particles (mean particle diameter of 20 nm) and is deionized. According to the manufacturer, however, the stock solution contains 0.04 wt % of Na_2SO_4. Bindzil 9950 is composed of larger particles (mean particle diameter of 60 nm) and is alkali-stabilized with 0.1 wt % of Na_2O.

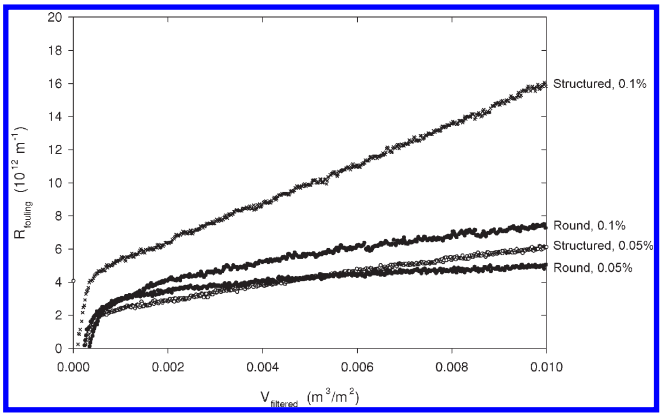

Figure 6. Increase in fouling resistance in a single filtration cycle at 70 L/h·m^2 for structured and round fibers with 0.05 and 0.1 wt % Ludox-TMA feed solution.

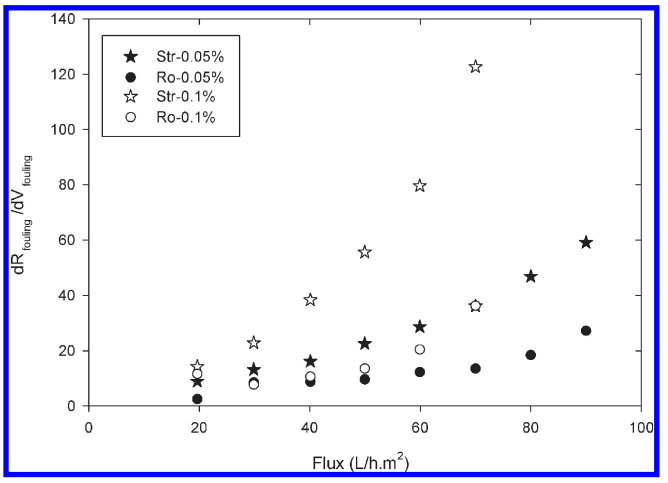

Figure 7. Fouling rate as a function of permeate flux, calculated as the slope of the $dR_{fouling}$ versus $dV_{filtered}$ plot (Figure 6) between $V_f = 0.006$ and 0.01 m^3/m^2.

The particle deposition with these two silica sols was investigated under two conditions: permeate flux of 70 L/h·m^2, with a 0.1 wt % feed concentration, and permeate flux of 20 L/h·m^2, with a 0.9 wt % feed concentration. It was observed that the deposition of the two sols followed different patterns. Figures 8 and 9 display the NMR images at different times of filtration together with the resistance increase as a function of filtrate volume. We must keep in mind that the images are recorded from the uppermost part of the fiber, whereas the resistance of the fouling layer reflects the whole fiber. In filtrations with hollow fibers, TMP, and therefore the deposit thickness, often varies throughout the length of the fiber because of the pressure drop in the fiber lumen.[15]

During the filtration of the Bindzil sol, there is a homogeneous deposition of the cake throughout the surface of the structured fiber (Figures 8 and 9). The thickness of the cake is similar for both structured and round fibers at fluxes of 20 and 70 L/h·m^2. The thicker cake at 20 L/h·m^2 is due to the higher feed concentration.

During the filtration of the Ludox sol, within the grooves, the deposit is more concentrated than on the fins and than the deposit on the round fibers. At 20 L/h·m^2, the deposit fills the whole groove starting from the first images, whereas at 70 L/h·m^2, it starts from the bottom of the groove and gradually fills it up. The deposition on the fins of the structured fiber and that on the round fiber appear to be much looser than that within the grooves. We must note that the calibrations for the particle concentration of the two sols with respect to the proton relaxation rates were different. Therefore, the intensities of the cake layer in the Ludox and Bindzil filtrations cannot be directly compared.

In a dead-end filtration, the material balance for the filtered particles is

$$\frac{\partial \phi}{\partial t} = \frac{\partial}{\partial x}\left[D(\phi)\frac{\partial \phi}{\partial x} - J\phi\right] \quad (1)$$

where ϕ denotes the particle volume fraction, $D(\phi)$ is the diffusion coefficient, J is the permeate flux, and x is the coordinate perpendicular to the membrane surface.

The concentration-dependent diffusion coefficient, $D(\phi)$, can be estimated using the generalized Stokes−Einstein equation

$$D(\phi) = \frac{V_p}{6\pi\mu a H(\phi)}\frac{d\Pi}{d\phi} \quad (2)$$

where V_p is the volume of the suspended particle, μ is the viscosity of the medium, a is the particle radius, $H(\phi)$ is the Happel function (see the Appendix), and Π is the osmotic pressure. The details of the osmotic pressure calculation are given in the Appendix.

Equation 1 was solved for the evolution of the concentration polarization (CP) layer using MATLAB. The following boundary and initial conditions were used

$$\text{at } x = 0,\ \phi(0,t) = \phi_{wall}$$

$$\text{at } x = \infty,\ \phi(\infty,t) = \phi_{bulk}$$

$$\text{at } t = 0,\ \phi(x,0) = \phi_{bulk}$$

where ϕ_{wall} is the maximum stable colloid concentration, which corresponds to the maximum osmotic pressure, or equivalently zero diffusivity. The time for the wall concentration to reach the maximum value of ϕ_{wall} is found to be negligible with respect to the time it takes to form a steady-state polarization layer based on the solution of eq 1 using a rate of concentration increase boundary condition at the wall. Also, at the time the wall concentration reaches ϕ_{wall}, the concentration away from the wall is assumed to be still the bulk concentration. After the formation of the concentration polarization layer, with continued filtration a cake layer starts to grow on the membrane wall, accompanied by a polarization layer on top of the cake.

At steady state, the convective transport is equal to the diffusive back transport. In Table 2, the steady-state thickness of the polarization layers is given. For all cases, the thicknesses are on the order of the convolutions of the structured fibers and would immediately fill the grooves of these fibers from the beginning of the filtration. However, the structures of the polarization layers of the two sols are quite different (Figure 10). For the Bindzil sol, the polarization layer is highly concentrated throughout its whole thickness. For 20 L/h·m^2, the total resistance of the polarization layer is estimated as 1.75×10^{12} m^{-1} using the Kozeny−Carman equation. This resistance is about the same magnitude as the intrinsic membrane resistance (1.55×10^{12} m^{-1}). The Ludox polarization layer, despite its high thickness, has very low concentrations in the majority of its thickness. The resistance of this dilute layer that extends throughout the groove is about two orders of magnitude smaller than the intrinsic membrane resistance (2.35×10^{10} m^{-1}). Consequently, when the filtration of the Bindzil sol starts, the polarization layer that forms immediately creates an imbalance between the total resistance in the grooves and that on the fins of the fiber. When there is such an imbalance, the total flow will be regulated such that more of it permeates through the low-resistance regions and less through the high-resistance regions. This self-regulation of the permeate flow acts toward equalizing the resistance throughout the surface because more will deposit on the initially lower resistance regions and vice versa. This results in a homogeneous cake thickness everywhere on the surface of the fiber.

For Ludox, with the polarization layer filling the grooves, the resistance is still essentially the same everywhere on the fiber because of the low resistance of this dilute polarization layer. As a result, equal amounts of permeate flow through the complete surface of the fiber. However, within the groove, the concentration is higher than that in the bulk, and as the groove is filled to the

(15) Yoon, S.; Lee, S.; Yeom, I.-T. Experimental verification of pressure drop models in hollow fiber membrane. *J. Membr. Sci.* **2008**, *310*, 7–12.

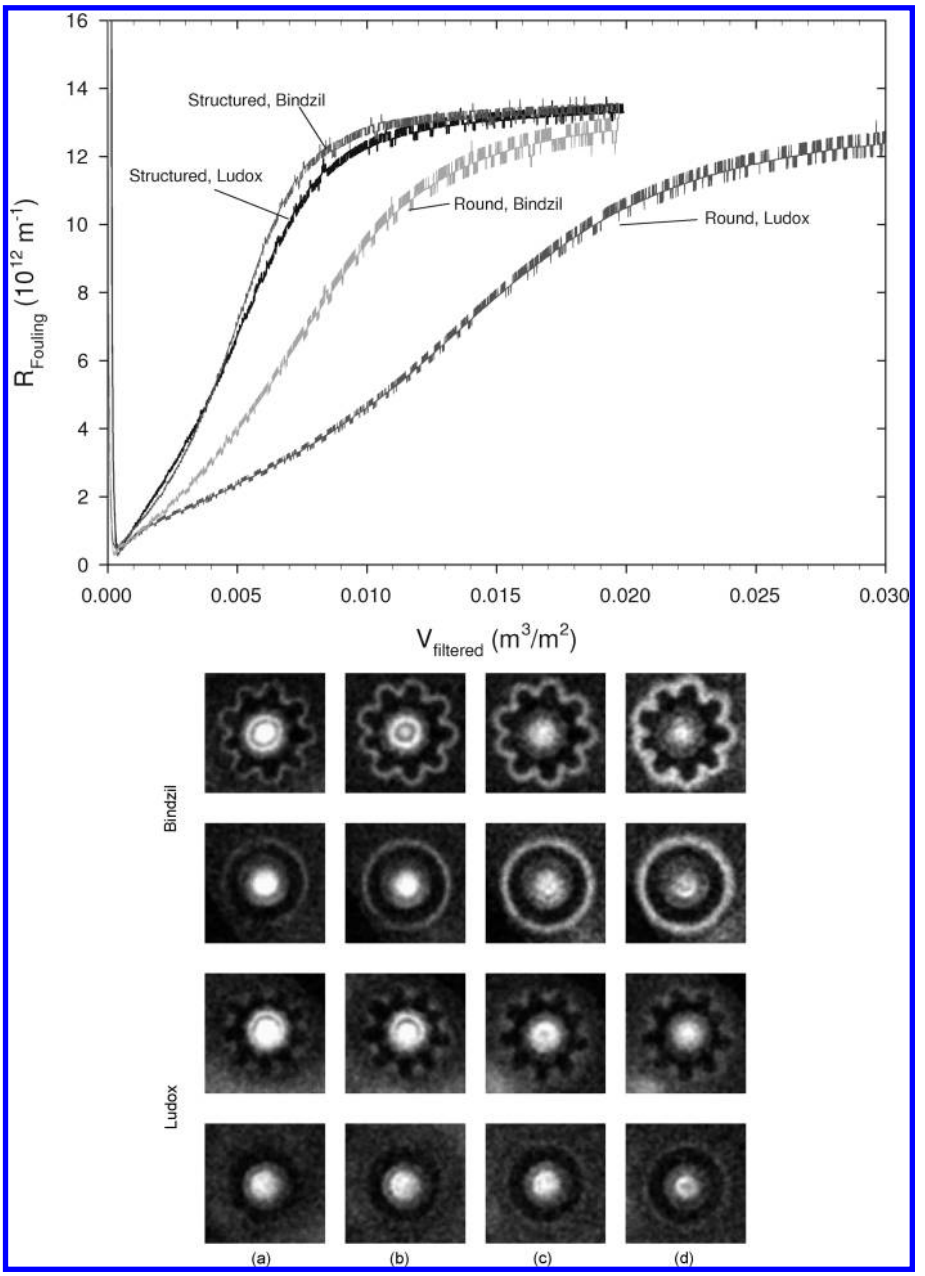

Figure 8. Particle deposition on structured and round fibers at 20 L/h·m^2 with 0.9 wt % Ludox and Bindzil sols. Images are from V_f = 0.0035 (a), 0.007 (b), 0.0125 (c), and 0.018 m^3/m^2 (d).

top, the total thickness of the CP layer for the bottom of the groove is twice that of the fins. Therefore, the concentration gradient for back diffusion is lower compared with that for the fins. As a result, the convective flow due to permeation is more dominant over back diffusion, and the deposit is more concentrated. Because the inhomogeneities in cake thickness and porosity create an imbalance between the different locations, the flow will start to be self-regulated in this case as well. However, for whatever the amount that flows through the grooves, the back diffusion will be less compared with that on the fins, which keeps the initial deposit trapped within the grooves and allows further deposition on and compression of this layer.

At 20 L/h·m^2, the deposit in the grooves is looser than that at 70 L/h·m^2. At 70 L/h·m^2, convective flow is more dominant over back diffusion, and the deposition in the grooves starts first from regions where the concentration gradient is lowest, that is, the bottom of the grooves, because the polarization layer does not fill the groove totally. As more cake deposits, the polarization layer starts to fill the whole groove, and the deposition moves on to fill most of the groove.

In flux-stepping experiments and NMR filtrations, we mostly see a steeper resistance increase with structured fibers. For the Bindzil sol, where the cake thickness and porosity appear similar in both fibers, this is attributed to the fact that the effective filtration area, which is that of the membrane and the cake layer on top, changes as the cake deposits.[16] For the round fibers, as more cake deposits, the area for filtration increases. For the structured fibers, with the grooves filled, soon the effective area becomes much less. Table 3 illustrates the change in membrane

(16) Belfort, G.; Davis, R. H.; Zydney, A. L. The behavior of suspensions and macromolecular solutions in crossflow microfiltration. *J. Membr. Sci.* **1994**, *96*, 1–58.

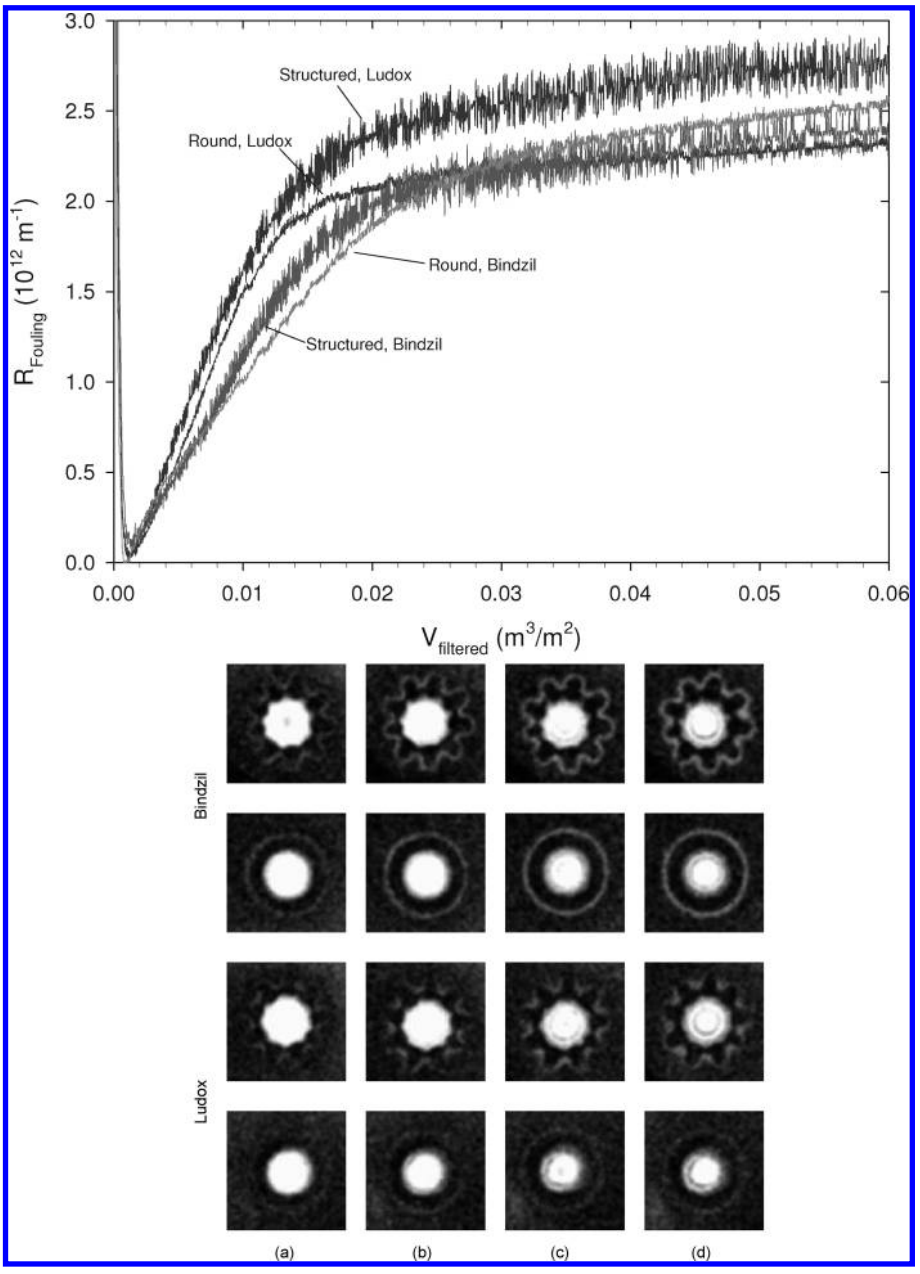

Figure 9. Particle deposition on structured and round fibers at 70 L/h·m^2 with 0.1 wt % Ludox and Bindzil sols. Images are from V_f = 0.01 (a), 0.02 (b), 0.04 (c), and 0.06 m^3/m^2 (d).

Table 2. Steady-State Concentration Polarization Layer Thickness for the Four Feed Solutions, Found by Solving eq *1* with the Transient Term Equal to Zero and δ_{cp} As the Distance *x* from the Membrane Where $\phi = \phi_{bulk}$

feed	δ_{cp} (μm)
70 L/h·m^2, 0.1 wt % Ludox	65
70 L/h·m^2, 0.1 wt % Bindzil	57
20 L/h·m^2, 0.9 wt % Ludox	190
20 L/h·m^2, 0.9 wt % Bindzil	130

area, and the resulting effective flux for the round and structured fibers. Assuming constant specific cake resistance, the ratio of the fouling resistances in the structured and round fibers is estimated in the last column and compared with the actual ratio observed. For the Bindzil sol, the estimate fits the actual values quite well. However, for the Ludox sol, the fouling resistance on the structured fibers is more than twice the resistance on the round fibers, which is much more than the value estimated solely based on the changing effective membrane area. This inconsistency is because in the grooves of the structured fibers, the cake is denser than that on the round fiber, and the higher specific resistance of this cake further increases its resistance.

Flux-Stepping Experiments with Sodium Alginate. With a 20 ppm sodium alginate feed solution, two distinct fouling behaviors were observed for the structured and round fibers (Figure 11). In the structured fiber, at fluxes >20 L/h·m^2, the resistance at the end of a filtration cycle is constant irrespective of the flux, whereas in the round fiber it increases with increasing flux. Also, in the structured fiber there is almost no irreversible fouling, whereas the round fiber starts to foul irreversibly from 70 L/h·m^2 on. The retention was similar for both fibers (Figure 12) and increased with increasing flux until 60 L/h·m^2, after which a maximum was reached around 90%. Although the low retention at 20 L/h·m^2 can partly explain the increasing

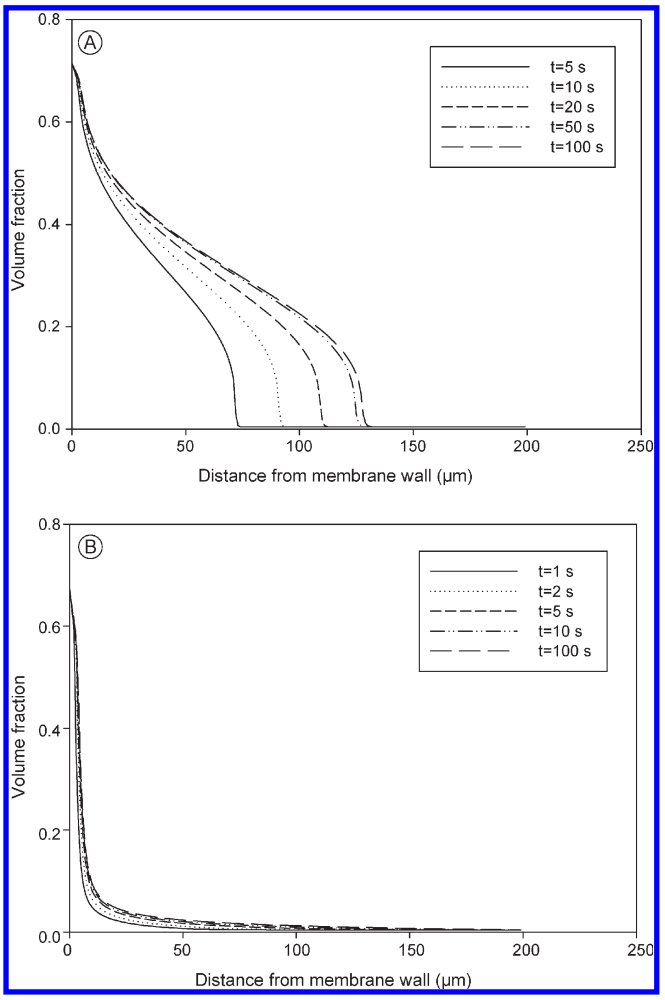

Figure 10. Formation of the concentration polarization layer during the filtration of 0.9 wt % Bindzil sol (a) and Ludox sol (b) at 20 L/h·m^2.

Table 3. Estimated and Experimentally Observed Ratios of Resistances of the Structured-to-Round Fibers[a]

0.9 wt % Bindzil at 20 L/h·m^2						
	A/A_0		J_{eff}		R_{str}/R_{ro}	
V_f	Str	Ro	Str	Ro	estimated	actual
0.0035	1.00	1.14	20.00	17.50	1.14	1.63
0.007	0.99	1.19	20.20	16.80	1.20	1.69
0.011	0.97	1.23	20.60	16.30	1.26	1.27
0.015	0.96	1.26	20.80	15.90	1.31	1.08
0.019	0.94	1.33	21.30	15.00	1.42	1.06
				average:	1.27	1.35
0.9 wt % Ludox at 20 L/h·m^2						
	A/A_0		J_{eff}		R_{str}/R_{ro}	
V_f	Str	Ro	Str	Ro	estimated	actual
0.0035	0.85	1.00	24.40	20.00	1.22	2.41
0.007	0.85	1.07	23.50	18.70	1.26	3.19
0.011	0.87	1.10	23.00	18.20	1.26	2.44
0.015	0.87	1.17	23.00	17.10	1.35	1.67
0.019	0.85	1.14	23.50	17.50	1.34	1.35
				average:	1.29	2.21

[a] A is the effective area for filtration after cake deposition, A_0 is the initial clean membrane area, and J_{eff} is the effective flux through the altered membrane area, A.

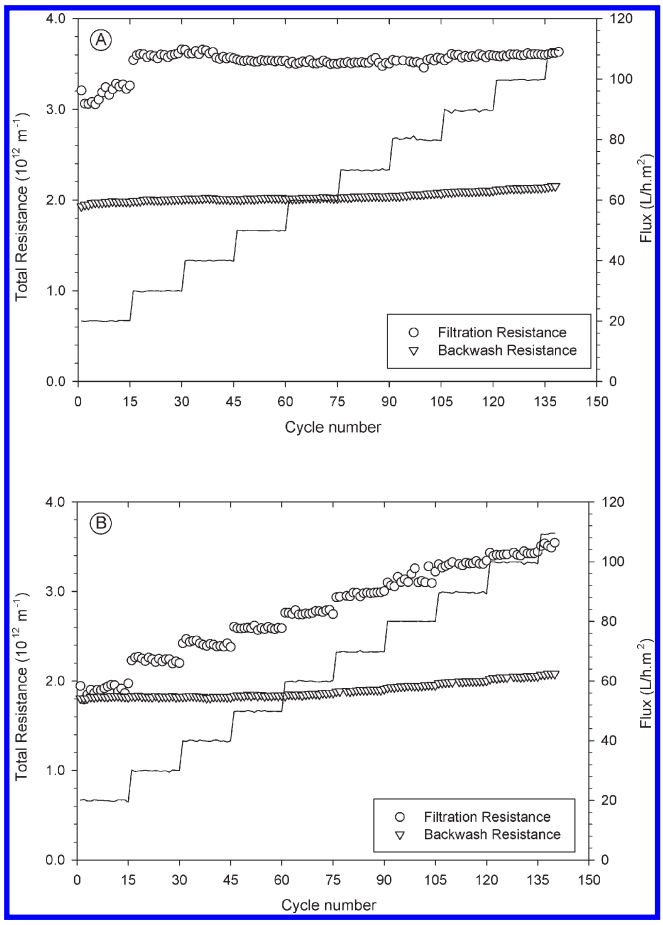

Figure 11. Flux-stepping experiments with 20 ppm sodium alginate: (a) structured fibers and (b) round fibers.

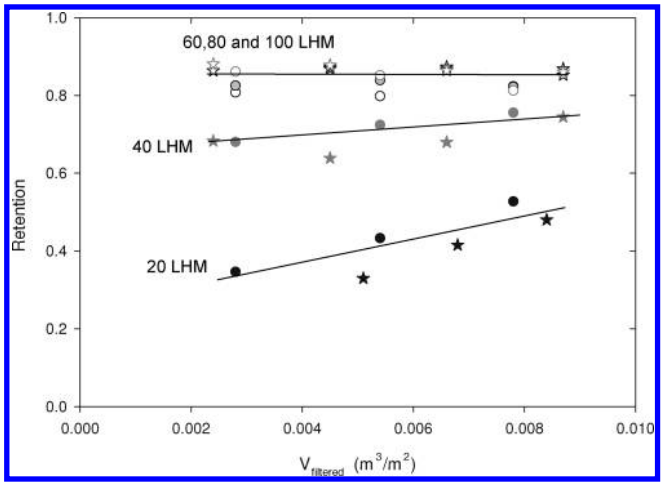

Figure 12. Sodium alginate retention of the fibers: Stars: structured fibers; Circles: round fibers.

resistance after this flux for both of the fibers, this cannot be the only reason for the difference between the two kinds of fibers since the retention is similar. Figure 13 shows the fouling resistance as a function of filtered volume for three different fluxes for the structured and round fibers. For the structured fiber, the resistance rises in a similar way at all fluxes, whereas in the round fiber, the rise is slower at low fluxes and gets faster with increasing flux.

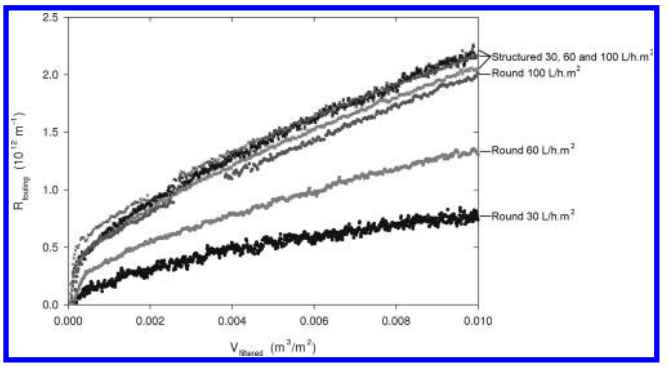

Figure 13. Increase in fouling resistance in separate sodium alginate filtration cycles at 30, 60, and 100 L/h·m^2 for the structured and round fibers.

Sodium alginate is a mixture with a broad size distribution (10−100 nm).[8] Within this broad distribution, there are small molecules with high diffusivities and large molecules with low diffusivities. Because of the difference in back diffusion of these different size fractions, they will be fractionated in the deposited cake with larger molecules closer to the membrane and smaller ones closer to the bulk.[8,17] At low fluxes, most of the small alginates will be loosely packed at the cake−bulk interface. As flux increases, the permeate drag will start to be dominant over back diffusion also for the smaller fractions, and the cake will be in a more compressed state. This explains why the resistance increases with increasing flux in the round fibers.[8]

For the structured fiber, on the basis of the size range of the alginates, their negative surface charge, and the low ionic strength of the medium, we can consider sodium alginate filtration as a superposition of the NMR observations with the Ludox and Bindzil silica sols. In this case, the large alginate fractions form a high resistance polarization layer within the grooves, with small particles concentrated close to the bulk and in much lower concentrations further within the groove. The resistance of this polarization layer can be significant, as in the case of the Bindzil sol (based on the calculation of the CP layer concentration profile and the resistance of this layer, as was done for the silica sols (Figure 10)), giving rise to the self-regulation of the permeate flow, which continuously tends to equalize the resistance throughout the fiber's surface. The initial filling of the grooves is expected to be similar at all fluxes, which explains the invariant resistance increase behavior at all fluxes. The self-regulating flow can create differences in porosity of the deposit on different parts of the fiber. In the grooves, the deposit is probably looser and thicker, whereas toward the fins, the porosity and thickness decrease, whereas the resistances are equal on both parts. The better reversibility of fouling can be attributed to the looseness of the majority of the deposit, which would make it easier to remove.

Conclusions

The fouling behavior of microstructured hollow fibers was investigated during constant flux filtrations of colloidal silica and sodium alginate. Additionally, NMR imaging was performed to study the deposition of two different silica sols. The deposition behavior was found to be different for the two sols of different particle size and solution ionic strength. For the smaller particle-sized sol in deionized solution (Ludox-TMA), the deposition within the grooves of the structured fibers was significantly higher than that on the fins. For the alkali-stabilized sol (Bindzil 9950), which had larger particles, the deposition was homogeneous throughout the surface of the structured fiber, and the thickness of the deposit was similar to that on the round fiber. This difference between the deposition behavior of the two sols was explained by differences in back diffusion, which create concentration polarization layers with different resistances. Both of the silica sols form polarization layers thick enough to fill all or most of the grooves in the structured fibers. Nevertheless, the polarization layer formed by the Ludox sol has very low resistance, whereas that of the Bindzil sol has a much higher resistance. This high resistance polarization layer that fills the grooves is considered to lead to quick flow regulation during the Bindzil sol filtration, which drives the filtration toward equalizing the resistance over the fiber surface. The Ludox particles are trapped at the bottom of the grooves because of equally continuing filtration through the grooves and the fins, which results in a lowered concentration gradient in the grooves and leads to reduced back diffusion.

The structured fibers showed better fouling reversibility than round fibers in sodium alginate filtrations. We explained this difference by considering the size-dependent deposition within the broad alginate size distribution. Filling of the grooves in the structured fibers with a high-resistance concentration polarization layer results in self-regulation of the permeate flow and consequently varying cake porosity throughout the fiber surface. Easier removal of the alginate deposit is thought to be caused by a looser structure, which is easier to remove than a compressed deposit on the round fibers.

As a conclusion, although initially, differences in particle deposition and cake porosity can be observed on the structured fibers, permeation will tend to be regulated to pass more through low resistance areas and less through high resistance areas. This will lead to an equalization of the resistances all along the structured fiber surface and therefore is not expected to be detrimental to the overall fouling performance. Furthermore, as seen in sodium alginate filtrations, this self-regulation can cause better fouling reversibility. On the whole, we observed that in dead-end filtrations, although the fouling resistances were somewhat higher for structured fibers, the fouling reversibility was better. In considering the higher resistances of the structured fibers, we must also note that because of the enhanced surface area, the actual permeate flow at a certain flux set point is 60% higher than that with the round fibers of equal length. This enhancement is more than the increased fouling resistance of these fibers and thus results in enhanced productivity.

Appendix: Calculation of Concentration-Dependent Diffusion Coefficient

The concentration-dependent diffusion coefficient of colloidal particles is estimated using the generalized Stokes−Einstein equation

$$D(\phi) = \frac{V_p}{6\pi\mu a H(\phi)} \frac{d\Pi}{d\phi} \quad (3)$$

where the Happel function, $H(\phi)$, is

$$H(\phi) = \frac{6 + 4\phi^{5/3}}{6 - 9\phi^{1/3} + 9\phi^{5/3} - 6\phi^2} \quad (4)$$

(17) van de Ven, W. J. C.; Pünt, I. G. M.; Kemperman, A. J. B.; Wessling, M. Unraveling ultrafiltration of polysaccharides with flow field flow fractionation. *J. Membr. Sci.* **2009**, *338*, 67–74.

Table 4. Data Used in Calculations

μ	0.001 Pa·s
A	6.51×10^{-21} J
ξ	−55 mV
d (for Na ions)[20]	0.23 nm
I (Ludox, 0.1 wt %)	0.006 mol/m^3
I (Ludox, 0.9 wt %)	0.055 mol/m^3
I (Bindzil, 0.1 wt %)	0.155 mol/m^3
I (Bindzil, 0.9 wt %)	1.363 mol/m^3

The osmotic pressure can be estimated by adding up the entropic, van der Waals and electrostatic contributions[5,6,18,19]

$$\Pi(\phi) = \Pi_{\text{entropy}} + \Pi_{\text{vanderWaals}} + \Pi_{\text{electrostatic}} \tag{5}$$

$$\Pi_{\text{entropy}} = \frac{3kT}{4\pi a^3}\phi\frac{1+\phi+\phi^2+0.67825\phi^3-\phi^4-0.5\phi^5-X\phi^6}{1-3\phi+3\phi^2-1.04305\phi^3} \tag{6}$$

where $X = 6.2028\exp\{[\phi_{\text{cp}}-\phi][7.9-3.9(\phi_{\text{cp}}-\phi)]\}$ with $\phi_{\text{cp}} = 0.74048$ for hexagonal close packing. k is the Boltzmann constant and T is the absolute temperature.

$$\Pi_{\text{vanderWaals}} = -\frac{z_n A}{48\pi a^3}\frac{\phi^3}{[\phi_{\text{cp}}-(\phi_{\text{cp}})^{1/3}\phi^{2/3}]^2} \tag{7}$$

where $z_n = 12$ for hexagonal close packing and A is the Hamaker constant (Table 4).

$$\Pi_{\text{electrostatic}} = \frac{\sqrt{6}}{A_{\text{h}}}f(D_1) \tag{8}$$

$$A_{\text{h}} = 2\sqrt{3}\left(a+\frac{D_1}{2}\right)^2 \tag{9}$$

$$D_1 = \left[\left(\frac{4\pi\sqrt{2}}{3\phi}\right)^{1/3}(a+d)-2a\right] \tag{10}$$

$$f(D_1) = \frac{1}{3}S_{\text{cell}}N_{\text{avo}}IkT(\cosh\Psi_{r_{\text{cell}}}-1) \tag{11}$$

$$S_{\text{cell}} = 4\pi r_{\text{cell}}^2 \tag{12}$$

$$r_{\text{cell}} = (2a+D_1)\left(\frac{3}{4\pi\sqrt{2}}\right)^{1/3} \tag{13}$$

$$\Psi_{r_{\text{cell}}} = \frac{A_1}{\beta}e^{\beta-\alpha}+\frac{(\xi^1\alpha-A_1)}{\beta}e^{-(\beta-\alpha)} \tag{14}$$

$$A_1 = \frac{\xi^1\alpha e^{-2(\beta-\alpha)}}{\frac{\beta-1}{\beta+1}+e^{-2(\beta-\alpha)}} \tag{15}$$

$$\xi^1 = \frac{ez\xi}{kT} \tag{16}$$

where d is the distance to the surface of shear, N_{avo} is Avogadro's number, I is the ionic strength, κ^{-1} is the Debye length, $\alpha = \kappa(a+d)$, $\beta = \kappa r_{\text{cell}}$, e is the elementary charge, z is the valence of the ions in solution, and ξ is the zeta potential.

(18) Bowen, W. R.; Jenner, F. Dynamic ultrafiltration model for charged colloidal dispersions: A wigner-seitz cell approach. *Chem. Eng. Sci.* **1995**, *50*, 1707–1736.

(19) Sarkar, B.; DasGupta, S.; De, S. Prediction of permeate flux during osmotic pressure-controlled electric field-enhanced cross-flow ultrafiltration. *J. Colloid Interface Sci.* **2008**, *319*, 236–246.

(20) Bowen, W. R.; Williams, P. M. The osmotic pressure of electrostatically stabilized colloidal dispersions. *J. Colloid Interface Sci.* **1996**, *184*, 241–250.